Free vibrations analysis of cracked variable stiffness composite plates by the eXtended Ritz method

A. Milazzo[1]

[1]Department of Engineering, University of Palermo, Viale delle Scienze, Bldg 8, 90128 Palermo - Italy ,
alberto.milazzo@unipa.it

Abstract

Variable stiffness composite laminates show advantageous structural features related to their enlarged design space. They are attractive candidates for advanced engineering applications where the assessment of static and dynamic behaviour and strength in presence of cracks is often required. In the present work, a single-domain extended Ritz formulation is proposed to study the free vibrations of cracked variable stiffness composite plates. The plate model is based on the first-order shear deformation theory whose primary variable, i.e. displacements and rotations, are approximated via a set of orthogonal polynomial trial functions enriched with a set of special crack functions. These functions are able to inherently account for crack opening and crack tip singular fields. The plate governing equations are deduced by the stationarity of the energy functional and the formulation has been implemented in a computer code. The method has been validated by comparing the present results with literature solutions for cracked isotropic plates and uncraked variable stiffness plates as, to the best of author's knowledge, no data on cracked variable stiffness plates free vibrations are available. An explicative and representative study on the free vibrations of variable angle tow composite laminates is finally presented with the aim of illustrating the approach capabilities, providing benchmarck results and identifying distinctive features and opportunities of the variable stiffness concept for the design of advanced damage tolerant structures. **Keywords:** *Variable stiffness composites, Cracked plates, Free vibrations, Extended Ritz method, X-Ritz method.*

1 Introduction

Recent developments in manufacturing technology [1] have made possible the implementation of an innovative design concept based on variable stiffness composite structures whose application in aerospace, automotive and naval applications appears very attractive. Indeed, it is proved that such structures can exhibit better structural behaviour with respect to the constant stiffness case [2]. This structural performances improvement is strictly associated with the appropriate design of the composite material and laminate layup. Actually, it is possible to take advantage from the extension of the material design space obtained through the variability of the fibre deposition angle, as in the variable angle tow technology, or the variability of material mixtures, as in the functionally graded materials case. Looking at advanced engineering application, buckling and dynamic structural performances need to be accurately taken into account in the structural design. Additionally, for fail safe or damage tolerant design requirements the presence of cracks need often to be considered, as cracks alter the structural response sometimes leading to unexpected or critical safety issues. Consequently it is crucial to develop appropriate analysis and design tools for variable stiffness composite plates and shells, which are the usual structural components in engineering applications. In this framework, due to the complexity of the problem, the development of numerical models and solutions is mandatory.

Focusing on the structural dynamics of composite variable stiffness plates, the literature survey returns that the finite element method has been extensively employed to investigate the linear free vibrations problen using the classical lamination theory (CLPT) [3], the first order shear deformation theory (FSDT) with both equivalent single layer [4, 5, 6, 7, 8] and layerwise [9] approach, the third order shear deformation theory (TSDT) [10], high order plate theories (HODT) [11] and layerwise 3D models [12]. Finite elements have been also employed for nonlinear free vibrations analysis [13, 14]. For linear free vibrations analysis, alternative methods have been proposed by Daraei and Hatami [15], who employed a semi-analytical finite strip method in the framework of the CLPT, and by Nie et al. [16], who used the CLPT and a complex fourier series solution. Heydarpour and Aghdam [17] investigated the transient response via 3D differential quadrature. The Ritz method has been also applied to study the free vibrations of variable stiffness plates modeled by CLPT [18, 19] and by variable kinematics plate theories [20]. All the works reported in the literature deal with *uncracked* variable stiffness plates and, to the best of the author's knowledge, no methods and solutions for the free vibrations analysis of cracked variable stiffness composites have been proposed. This represents a gap of insight and know-how in the field of this emerging structural concept.

In view of the above described outline and with the aim to contribute to develop alternative tools useful for the fail safe and damage tolerant design, in this paper the so-called X-Ritz method is proposed for the free vibrations analysis of cracked, variable stiffness plates. The X-Ritz method has been presented by the author and co-workers in previous works [21, 22, 23] and it has been successfully applied to variable stiffness cracked plate buckling analysis [24]. It consists of a single-domain FSDT plate Ritz formulation, which inherently accounts for the presence of embedded or edge through-the-thickness cracks. This is achieved by expressing the problem primary variables via a trial functions set consisting of orthogonal polynomials and special functions, which able to represent crack discontinuity and singular behaviour. The objectives of the present work are: (*i*) to validate the X–Ritz method applicability to variable stiffness plate free vibrations analysis, verifying its accuracy and effectiveness; (*ii*) to study the effects of cracks on the free vibrations behaviour of VAT plates; (*iii*) to provide benchmark results for future works as, to the best of the author's knowledge, this is the first time free vibrations of cracked variable stiffness plates are investigated.

The paper is organised as follows. The cracked plate formulation, the X-Ritz approximation and the corresponding plate governing equations are briefly presented in Sec.2, referring to previous works for the derivation details so as to keep the article short. Next, the validation of the proposed method and original results are presented and discussed in Sec.3, followed by the concluding remarks in Sec.4.

2 Formulation

Consider a variable stiffness quadrilateral plate referred to a Cartesian coordinate system $Ox_1x_2x_3$ whose x_1 and x_2 axes lay in the plate reference plane Ω and the x_3 axis is directed along the thickness. The plate contains a straight, through-the-thickness crack. To deal with general quadrilateral geometries, let us introduce the natural coordinate system $O\xi\eta$, which maps the square domain $[-1,1]\times[-1,1]$ onto the plate mid-plane coordinates via standard bilinear shape functions [25]. Finally, a polar coordinates system $Or_k\theta_k$ is defined with origin at each crack tip. Fig. 1 shows a sketch of the plate geometry and the reference systems introduced .

2.1 Variational statement

In the framework of the first order shear deformation theory [26], assuming that the strain–displacement relationships, the constitutive relationships and the kinematical boundary conditions are fulfilled, the

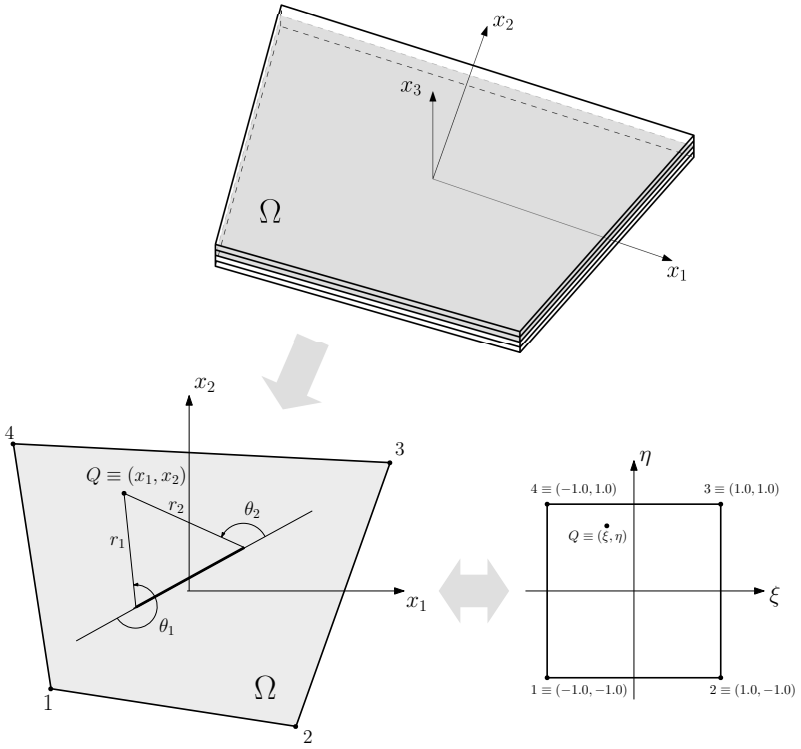

Figure 1: Plate geometry and reference systems.

governing equations for plate vibrations are obtained by the stationarity of the following functional with respect to the primary variable , namely the translational displacements vector $\boldsymbol{u} = \{u_1 \;\; u_2 \;\; u_3\}^T$ and the transverse section rotations vector $\boldsymbol{\psi} = \{\psi_1 \;\; \psi_2\}^T$ [27]

$$\begin{aligned}\Pi = \int_\Omega \frac{1}{2}\Big[&(\boldsymbol{\mathscr{D}}_p \boldsymbol{u})^T \boldsymbol{A}\, \boldsymbol{\mathscr{D}}_p \boldsymbol{u} + (\boldsymbol{\mathscr{D}}_p \boldsymbol{u})^T \boldsymbol{B}\, \boldsymbol{\mathscr{D}}_p\, \boldsymbol{\mathscr{L}} \boldsymbol{\psi} + (\boldsymbol{\mathscr{D}}_p \boldsymbol{\mathscr{L}} \boldsymbol{\psi})^T \boldsymbol{B}\, \boldsymbol{\mathscr{D}}_p \boldsymbol{u} + \\ &(\boldsymbol{\mathscr{D}}_p \boldsymbol{\mathscr{L}} \boldsymbol{\psi})^T \boldsymbol{D}\, \boldsymbol{\mathscr{D}}_p \boldsymbol{\mathscr{L}} \boldsymbol{\psi} + (\boldsymbol{\mathscr{D}}_n \boldsymbol{u} + \boldsymbol{\mathscr{L}} \boldsymbol{\psi})^T \boldsymbol{G}\; (\boldsymbol{\mathscr{D}}_n \boldsymbol{u} + \boldsymbol{\mathscr{L}} \boldsymbol{\psi}) \Big] d\Omega - \\ \omega^2 \int_\Omega \frac{1}{2} &\Big[\; \boldsymbol{u}^T \boldsymbol{J}_0 \boldsymbol{u} + \boldsymbol{u}^T \boldsymbol{J}_1 \boldsymbol{\psi} + \boldsymbol{\psi}^T \boldsymbol{J}_1^T \boldsymbol{u} + \boldsymbol{\psi}^T \boldsymbol{J}_2 \boldsymbol{\psi} \;\Big] d\Omega\end{aligned} \tag{1}$$

where ω is the vibrational natural angular frequency and the strain displacement operators $\boldsymbol{\mathscr{D}}_p$, $\boldsymbol{\mathscr{D}}_n$ and $\boldsymbol{\mathscr{L}}$ are introduced as

$$\boldsymbol{\mathscr{D}}_p = \begin{bmatrix} \dfrac{\partial}{\partial x} & 0 & 0 \\ 0 & \dfrac{\partial}{\partial y} & 0 \\ \dfrac{\partial}{\partial y} & \dfrac{\partial}{\partial x} & 0 \end{bmatrix}, \qquad \boldsymbol{\mathscr{D}}_n = \begin{bmatrix} 0 & 0 & \dfrac{\partial}{\partial x} \\ 0 & 0 & \dfrac{\partial}{\partial y} \\ 0 & 0 & 0 \end{bmatrix} \qquad \boldsymbol{\mathscr{L}} = \begin{bmatrix} 1 & 0 \\ 0 & 1 \\ 0 & 0 \end{bmatrix} \tag{2}$$

In the Eq. (1), $\boldsymbol{A}$, $\boldsymbol{B}$, $\boldsymbol{D}$ and $\boldsymbol{G}$ are the extensional, bending–extension coupling, bending and shear stiffness matrices, respectively. It is worth nothing that for variable stiffness plate they are function of the in-plane coordinates x_1 and x_2. Their definition is given in A, whereas details for their evaluation in the variable angle tow (VAT) specific case are given in C. Also, in the Eq. (1), $\boldsymbol{J}_0$, $\boldsymbol{J}_1$, $\boldsymbol{J}_2$ are the mass moments of inertia matrices, whose expressions are given in B.

2.2 X–Ritz model

The solution of the linear vibration problem for cracked plates, defined by the stationarity of the potential Π in Eq. (1), is achieved by the X–Ritz method [21, 23]. It is based on the primary variable approximation via a pb2-Ritz scheme [28] enriched by means of special functions able to describe the crack opening and the crack tip fields [29, 30, 31, 32]. For an embedded crack, at the point of natural coordinates (ξ, η) and corresponding polar coordinates (r_1, θ_1) and (r_2, θ_2), the primary variable $\chi \in \{u_1, u_2, u_3, \psi_1, \psi_2\}$ is approximated as

$$\begin{aligned}\chi = f_\chi(\xi,\eta) \sum_{m=0}^{M}\sum_{n=0}^{N} \mathscr{L}_m(\xi)\mathscr{L}_n(\eta) C^{\langle 0\rangle}_{\chi mn} + \\ g_\chi(\xi,\eta) \sum_{m=1}^{N_c}\sum_{n=0}^{m} \Bigg\{ r_1{}^{\frac{2m-1}{2}} \cos\left(\tfrac{2n+1}{2}\theta_1\right) C^{\langle 1\rangle}_{\chi mn} + r_2{}^{\frac{2m-1}{2}} \cos\left(\tfrac{2n+1}{2}\theta_2\right) C^{\langle 2\rangle}_{\chi mn} + \\ \sqrt{r_2{}^3}\sin^2\left(\frac{\theta_2}{2}\right) r_1{}^{\frac{2m-1}{2}} \sin\left(\tfrac{2n+1}{2}\theta_1\right) C^{\langle 3\rangle}_{\chi mn} + \\ \sqrt{r_1{}^3}\sin^2\left(\frac{\theta_1}{2}\right) r_2{}^{\frac{2m-1}{2}} \sin\left(\tfrac{2n+1}{2}\theta_2\right) C^{\langle 4\rangle}_{\chi mn} \Bigg\}\end{aligned} \tag{3}$$

where $\mathscr{L}_j(\zeta)$ is the j–th order Legendre polynomial of the coordinate ζ and the $C^{\langle k\rangle}_{\chi mn}$ ($k \in \{0,1,2,3,4\}$) are the unknown Ritz coefficients. According to the pb2 Ritz, the functions $f_\chi(\xi,\eta)$ and $g_\chi(\xi,\eta)$ of Eq. (3) ensure the fulfillment of the kinematical boundary conditions; they are defined as

$$f_\chi(\xi,\eta) = (1+\xi)^{q_1}(1-\xi)^{q_2}(1+\eta)^{q_3}(1-\eta)^{q_4} \tag{4}$$

$$g_\chi(\xi,\eta) = (1-\xi^2)(1-\eta^2) \tag{5}$$

where the exponents q_i depend on the plate edges kinematical boundary conditions and are set as indicated in Table 1. The approximation of Eq. (3) consists of two contributions: *i*) the first series contains regular functions able to describe the global plate behaviour disregarding crack opening and crack tip singularities;

Edge	Free	Constrained
$(1+\xi)=0$	$q_1=q_2=q_3=q_4=0$	$q_1=1;\ q_2=q_3=q_4=0$
$(1-\xi)=0$	$q_1=q_2=q_3=q_4=0$	$q_2=1;\ q_1=q_3=q_4=0$
$(1+\eta)=0$	$q_1=q_2=q_3=q_4=0$	$q_3=1;\ q_1=q_2=q_4=0$
$(1-\eta)=0$	$q_1=q_2=q_3=q_4=0$	$q_4=1;\ q_1=q_2=q_3=0$

Table 1: Exponents values in Eq.(4) to constrain the primary variable $\chi \in \{u_1, u_2, u_3, \psi_1, \psi_2\}$.

i) the second series contains enrichment terms, which describe the crack opening and the singular fields at the crack tips. It is worth noting that the enrichment functions are forced to zero on the plate edges via the boundary function $g_\chi(\xi,\eta)$ and that the plate kinematical conditions are then fullfilled by properly setting the boundary function $f_\chi(\xi,\eta)$. For more details on the characteristics of the enrichment terms refer to [33, 21, 22].

Similarly, for edge cracks that presents a single tip the X-Ritz approximation is given by

$$\begin{aligned}\chi = f_\chi(\xi,\eta)\sum_{m=0}^{M}\sum_{n=0}^{N}\mathscr{L}_m(\xi)\mathscr{L}_n(\eta)C^{\langle 0\rangle}_{\chi mn}+ \\ g_\chi(\xi,\eta)\sum_{m=1}^{N_c}\sum_{n=0}^{m}\left\{r_1{}^{\frac{2m-1}{2}}\cos\left(\frac{2n+1}{2}\theta_1\right)C^{\langle 1\rangle}_{\chi mn}+\quad r_1{}^{\frac{2m-1}{2}}\sin\left(\frac{2n+1}{2}\theta_1\right)C^{\langle 3\rangle}_{\chi mn}\right\}\end{aligned} \tag{6}$$

where, to allow crack opening at the edge, the function g_χ is chosen as in Eq. (4) setting to 0 the exponent q_k associated with the edge intersected by the crack and to 1 all of the other exponents. Obviously, the trial function in Eqs. (3) and (6) can be used for uncracked plates by setting $N_c = 0$

In compact matrix form the introduced X-Ritz approximation is written as

$$\begin{Bmatrix}\boldsymbol{u}\\ \boldsymbol{\psi}\end{Bmatrix} = \begin{Bmatrix}u_1\\ u_2\\ u_3\\ \hdashline \psi_1\\ \psi_2\end{Bmatrix} = \left[\begin{array}{ccc:cc} \boldsymbol{\varphi} & \mathbf{0} & \mathbf{0} & \mathbf{0} & \mathbf{0}\\ \mathbf{0} & \boldsymbol{\varphi} & \mathbf{0} & \mathbf{0} & \mathbf{0}\\ \mathbf{0} & \mathbf{0} & \boldsymbol{\varphi} & \mathbf{0} & \mathbf{0}\\ \hdashline \mathbf{0} & \mathbf{0} & \mathbf{0} & \boldsymbol{\varphi} & \mathbf{0}\\ \mathbf{0} & \mathbf{0} & \mathbf{0} & \mathbf{0} & \boldsymbol{\varphi}\end{array}\right] \begin{Bmatrix}\boldsymbol{X}_{u_1}\\ \boldsymbol{X}_{u_2}\\ \boldsymbol{X}_{u_3}\\ \boldsymbol{X}_{\psi_1}\\ \boldsymbol{X}_{\psi_2}\end{Bmatrix} = \left[\begin{array}{c:c} \boldsymbol{\Phi_u} & \mathbf{0}\\ \hdashline \mathbf{0} & \boldsymbol{\Phi_\psi}\end{array}\right]\boldsymbol{X} = \boldsymbol{\Phi X} \tag{7}$$

where $\boldsymbol{\varphi}$ is a row vector collecting the employed trial functions and $\boldsymbol{X}_\chi$ is the column vector collecting the unknown Ritz coefficients $C^{\langle j\rangle}_{\chi mn}$ being $j \in \{0,1,2,3,4\}$ for embedded cracks and $j \in \{0,1,3\}$ for edge cracks, respectively

By substituting the primary variable approximations Eq. (7) into Eq. (1), the discretized form of the functional Π is obtained. Its stationarity condition with respect to the unknown Ritz coefficients

[21, 22] provides the following plate free vibrations governing equations

$$\left(\boldsymbol{K} - \omega^2 \boldsymbol{M}\right) \boldsymbol{X} = \boldsymbol{0} \tag{8}$$

where

$$\boldsymbol{K} = \int_\Omega \begin{bmatrix} (\boldsymbol{\mathscr{D}}_p \boldsymbol{\Phi}_{\boldsymbol{u}})^T \boldsymbol{A} \boldsymbol{\mathscr{D}}_p \boldsymbol{\Phi}_{\boldsymbol{u}} + (\boldsymbol{\mathscr{D}}_n \boldsymbol{\Phi}_{\boldsymbol{u}})^T \boldsymbol{G} \boldsymbol{\mathscr{D}}_n \boldsymbol{\Phi}_{\boldsymbol{u}} & (\boldsymbol{\mathscr{D}}_p \boldsymbol{\Phi}_{\boldsymbol{u}})^T \boldsymbol{B} \boldsymbol{\mathscr{D}}_p \boldsymbol{\mathscr{L}} \boldsymbol{\Phi}_{\boldsymbol{\psi}} + (\boldsymbol{\mathscr{D}}_n \boldsymbol{\Phi}_{\boldsymbol{u}})^T \boldsymbol{G} \boldsymbol{\mathscr{L}} \boldsymbol{\Phi}_{\boldsymbol{\psi}} \\ (\boldsymbol{\mathscr{D}}_p \boldsymbol{\mathscr{L}} \boldsymbol{\Phi}_{\boldsymbol{\psi}})^T \boldsymbol{B} \boldsymbol{\mathscr{D}}_p \boldsymbol{\Phi}_{\boldsymbol{u}} + (\boldsymbol{\mathscr{L}} \boldsymbol{\Phi}_{\boldsymbol{\psi}})^T \boldsymbol{G}\, \boldsymbol{\mathscr{D}}_n \boldsymbol{\Phi}_{\boldsymbol{u}} & (\boldsymbol{\mathscr{D}}_p \boldsymbol{\mathscr{L}} \boldsymbol{\Phi}_{\boldsymbol{\psi}})^T \boldsymbol{D} \left(\boldsymbol{\mathscr{D}}_p \boldsymbol{\mathscr{L}} \boldsymbol{\Phi}_{\boldsymbol{\psi}}\right) + (\boldsymbol{\mathscr{L}} \boldsymbol{\Phi}_{\boldsymbol{\psi}})^T \boldsymbol{G}\ (\boldsymbol{\mathscr{L}} \boldsymbol{\Phi}_{\boldsymbol{\psi}}) \end{bmatrix} d\Omega \tag{9}$$

$$\boldsymbol{M} = \int_\Omega \begin{bmatrix} \boldsymbol{\Phi}_{\boldsymbol{u}}^T \boldsymbol{J}_0 \boldsymbol{\Phi}_{\boldsymbol{u}} & \boldsymbol{\Phi}_{\boldsymbol{u}}^T \boldsymbol{J}_1 \boldsymbol{\Phi}_{\boldsymbol{u}} \\ \boldsymbol{\Phi}_{\boldsymbol{\psi}}^T \boldsymbol{J}_1^T \boldsymbol{\Phi}_{\boldsymbol{u}} & \boldsymbol{\Phi}_{\boldsymbol{\psi}}^T \boldsymbol{J}_2 \boldsymbol{\Phi}_{\boldsymbol{\psi}} \end{bmatrix} d\Omega \tag{10}$$

The Eq. (8) is an homogeneous linear algebraic system whose eigenvalues provide the plate natural circular frequency ω and the corresponding eigenvectors describe the modal shapes in terms of the Ritz coefficients.

3 Numerical Results

A computer code based on the formulation outlined in Sec. 2 has been implemented. With reference to the numerical implementation of the method, it is remarked that the evaluation of the $\boldsymbol{K}$ and $\boldsymbol{M}$ matrices requires the computation of domain integrals whose integrand functions exhibit high gradients near the crack tips; considering that the method effectiveness relies on the accurate evaluation of the resolving system matrices, appropriate numerical integration schemes has been implemented as proposed in [23].

3.1 Convergence analysis and validation

Convergence analyses have been carried out to ascertain the behaviour of the proposed approach. To this aim, square plates having edge length $a = b = 1\,\mathrm{m}$ and two different thickness ratio, namely $h/a = 0.01$ and $h/a = 0.1$, have been considered assuming simply-supported and clamped boundary conditions applied to all of the edges (see Fig. 2 for plate geometry definition). Referring to the notation described in C, the plates have a $[\langle 90, 45\rangle/\langle 60, 30\rangle/\langle 90, 45\rangle]$ VAT layup with plies exhibiting the following properties in the orthotropic material reference system: $E_1 = 173.0\,\mathrm{GPa}$, $E_2 = E_3 = 7.2\,\mathrm{GPa}$, $G_{13} = G_{12} = G_{23} =$

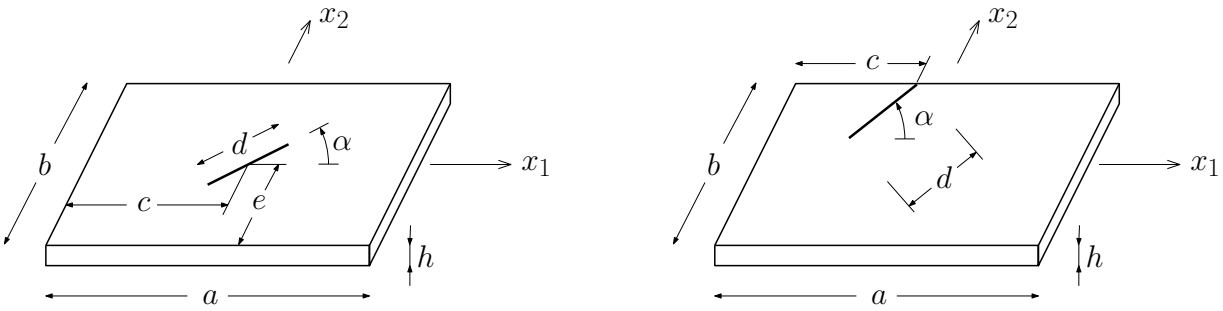

(a) Central crack (b) Edge crack

Figure 2: Cracked plate geometry.

3.76 GPa, $\nu_{12} = 0.29$ and $\rho = 1540\,\mathrm{kg\,m^{-3}}$, being E_i the Young's moduli, G_{ij} the shear moduli, ν_{ij} the Poisson's coefficients and ρ the material density. The approximation employed in the analyses consists of $N \times N$ regular trial functions and N_c enrichment functions for the modelization of the crack. Table 2 lists the results obtained for the first three nondimensional natural frequencies $\lambda = \omega \dfrac{a^2}{h}\sqrt{\dfrac{\rho}{E_1}}$ of the uncracked simply supported and clamped plates as the number N of the regular trial functions grows. In Table 2, available literature results [10, 16] are also reported for comparison and error appraisal. The obtained results show the capability of the approach to describe efficiently variable uncracked stiffness plate free vibrations as converged values are rapidly attained showing errors with respect to the literature data that not exceed 2%. Then, the case of cracked plates has been investigated and Table 3 lists the results for

Table 2: Nondimensional frequency parameter λ for the $[\langle 90, 45\rangle/\langle 60, 30\rangle/\langle 90, 45\rangle/]$ VAT square laminate.

	Simply-supported						Clamped					
	$h/a = 0.01$			$h/a = 0.1$			$h/a = 0.01$			$h/a = 0.1$		
N	Mode 1	Mode 2	Mode 3	Mode 1	Mode 2	Mode 3	Mode 1	Mode 2	Mode 3	Mode 1	Mode 2	Mode 3
4	3.32	8.19	13.78	2.74	5.02	7.25	7.20	48.65	52.50	4.09	6.64	8.08
6	3.18	5.59	9.39	2.64	4.27	6.69	6.88	9.90	16.53	3.97	5.42	7.43
8	3.13	5.21	8.47	2.60	4.19	6.56	6.77	8.84	13.23	3.95	5.35	7.38
10	3.11	5.12	8.35	2.58	4.16	6.51	6.71	8.67	12.73	3.95	5.34	7.38
12	3.10	5.09	8.33	2.58	4.15	6.50	6.70	8.63	12.63	3.95	5.33	7.38
14	3.09	5.07	8.32	2.57	4.14	6.49	6.69	8.62	12.60	3.94	5.33	7.38
16	3.09	5.06	8.32	2.57	4.14	6.49	6.69	8.61	12.59	3.94	5.33	7.38
Ref. [10]	3.11	5.09	8.36	2.59	4.15	6.53	6.71	8.61	12.60	3.94	5.32	7.38
Ref. [16]	3.12	5.14	8.47	—	—	—	6.75	8.64	12.72	—	—	—

simply supported square plates containing a central horizontal crack, namely $c/a = e/b = 0.5$ and $\alpha = 0°$, with length $d/a = 0.5$. The results show good convergence properties of the enrichment contribution evidencing also that the accuracy depends on the appropriate description of the plate global behaviour

via the regular trial functions contribution. It is remarked that no results have been found in the literature for the cracked variable stiffness plates free vibrations problem in order to extend the validation comparison also to this case. Generally, the data suggest that the method convergence properties appear insensitive

Table 3: Nondimensional frequency parameter λ for the simply supported square $[\langle 90, 45\rangle/\langle 60, 30\rangle/\langle 90, 45\rangle/]$ VAT laminate with central horizontal crack ($c/a = e/a = 0.5, d/a = 0.5$, $\alpha = 0°$).

	$h/a = 0.01$						$h/a = 0.1$					
	$N = 8$			$N = 16$			$N = 8$			$N = 16$		
N_c	Mode 1	Mode 2	Mode 3	Mode 1	Mode 2	Mode 3	Mode 1	Mode 2	Mode 3	Mode 1	Mode 2	Mode 3
1	2.93	5.09	8.44	2.83	4.96	8.30	1.84	3.50	3.94	1.78	3.40	3.89
2	2.68	4.77	5.36	2.55	4.57	5.20	1.79	3.24	3.91	1.76	3.20	3.87
3	2.07	4.57	5.02	2.01	4.47	4.92	1.77	3.19	3.88	1.74	3.18	3.85
4	2.02	4.49	4.68	1.98	4.42	4.61	1.76	3.19	3.87	1.74	3.17	3.85
5	2.01	4.44	4.66	1.97	4.40	4.60	1.76	3.18	3.87	1.73	3.17	3.84
6	2.01	4.41	4.64	1.97	4.38	4.60	1.76	3.18	3.87	1.73	3.17	3.84
7	2.00	4.40	4.64	1.97	4.37	4.60	1.75	3.18	3.86	1.73	3.17	3.84
8	2.00	4.38	4.64	1.97	4.37	4.60	1.75	3.18	3.86	1.73	3.17	3.84

to the thickness ratio. It is worth noting that the illustrated convergence studies are representative of the approach convergence features and they are supported and confirmed by an extensive validation numerical campaign whose results are not provided here for the sake of brevity.

Accuracy of the method has been investigated by comparing its solutions with results available in the literature or obtained by finite elements. Accordingly with the performed convergence analyses, the following results by the present method have been obtained by setting $N = 16$ and $N_c = 6$. Firstly, the free vibrations of uncracked VAT plates with the same geometrical characteristics and material properties as those used for the preceding convergence studies have been considered and the corresponding results compared with those of Ref. [10], which are based on a third order kinematic plate model. Tables 4 and 5 list the nondimensional natural frequencies λ for the $[\langle 0, 45\rangle/\langle -45, -60\rangle/\langle 0, 45\rangle]$, $[\langle 30, 0\rangle/\langle 45, 90\rangle/\langle 30, 0\rangle]$ and $[\langle 90, 45\rangle/\langle 60, 30\rangle/\langle 90, 45\rangle]$ VAT layups and different thickness ratios for simply-supported and clamped boundary conditions, respectively. There is good agreement between present and literature results; some appreciable differences appear for the higher modes of thick plates (however contained within 3%), which can be ascribed to the different kinematic models. As stated above, for cracked variable stiffness plates no free vibrations results are available and then the method accuracy and potentiality have been validated through its application to isotropic and orthotropic constant stiffness plates. An isotropic square plate

Table 4: Nondimensional frequency parameter λ for uncracked simply-supported square VAT laminates.

	$[\langle 0,45\rangle/\langle -45,-60\rangle/\langle 0,45\rangle]$				$[\langle 30,0\rangle/\langle 45,90\rangle/\langle 30,0\rangle]$				$[\langle 90,45\rangle/\langle 60,30\rangle/\langle 90,45\rangle]$			
	$h/a=0.01$		$h/a=0.1$		$h/a=0.01$		$h/a=0.1$		$h/a=0.01$		$h/a=0.1$	
Mode	Present	Ref. [10]	Present	Ref. [10]	Present	Ref. [10]	Present	Ref. [10]	Present	Ref. [10]	Present	Ref. [10]
1	3.36	3.38	2.74	2.77	2.91	2.91	2.45	2.47	3.09	3.11	2.57	2.59
2	5.55	5.57	4.41	4.42	4.76	4.75	3.96	3.99	5.06	5.09	4.14	4.15
3	9.06	9.06	6.52	6.61	7.99	7.98	6.26	6.33	8.32	8.36	6.49	6.53
4	10.11	10.14	6.91	6.91	10.67	10.67	6.65	6.72	10.19	10.30	6.62	6.66
5	12.44	12.53	7.90	7.99	12.06	12.08	7.82	7.91	11.93	12.08	7.73	7.79
6	13.83	13.91	9.87	9.86	12.33	12.34	8.66	8.79	13.16	13.23	9.01	9.08
7	16.17	16.29	10.17	10.29	16.02	16.05	10.27	10.45	15.73	16.56	10.31	10.53
8	19.63	20.16	10.73	10.99	16.47	16.60	10.86	11.10	16.82	17.08	10.69	10.84
9	20.98	21.35	11.81	12.09	21.49	22.10	11.22	11.47	20.35	20.91	11.52	11.68

Table 5: Nondimensional frequency parameter λ for uncracked clamped square VAT laminates.

	$[\langle 0,45\rangle/\langle -45,-60\rangle/\langle 0,45\rangle]$				$[\langle 30,0\rangle/\langle 45,90\rangle/\langle 30,0\rangle]$				$[\langle 90,45\rangle/\langle 60,30\rangle/\langle 90,45\rangle]$			
	$h/a=0.01$		$h/a=0.1$		$h/a=0.01$		$h/a=0.1$		$h/a=0.01$		$h/a=0.1$	
Mode	Present	Ref. [10]	Present	Ref. [10]	Present	Ref. [10]	Present	Ref. [10]	Present	Ref. [10]	Present	Ref. [10]
1	5.46	5.47	3.55	3.64	6.28	6.29	3.80	3.91	6.69	6.71	3.94	4.04
2	7.75	7.75	5.30	5.39	8.14	8.14	5.24	5.37	8.61	8.61	5.30	5.44
3	11.57	11.57	7.04	7.31	11.66	11.65	7.38	7.71	12.59	12.60	7.38	7.73
4	14.07	14.09	7.82	7.93	16.05	16.05	7.48	7.75	15.86	15.94	7.53	7.78
5	16.26	16.29	8.53	8.80	16.75	16.75	8.63	9.02	17.27	17.33	8.37	8.69
6	16.75	16.75	10.46	10.66	17.94	17.95	9.78	10.19	18.69	18.75	9.76	10.16
7	20.10	20.15	11.11	11.45	21.40	21.42	11.06	11.53	21.10	21.49	10.93	11.38
8	23.04	23.05	11.18	11.65	21.78	21.80	11.23	12.00	23.14	23.27	11.22	11.80
9	25.46	25.54	12.21	12.75	27.07	27.17	12.16	12.79	27.25	27.55	11.84	11.86

with Poisson's ratio $\nu = 0.3$ and thickness ratio $h/a = 0.1$ has been considered containing a central crack ($c/a = e/a = 0.5$) with different length ratios d/a and inclination α (see Fig 2a); two boundary conditions have been investigated, namely simply supported and cantilevered along the side orthogonal to the crack. The results obtained for the first five natural frequencies are listed in Table 6 where comparison with results from Ref. [32] is proposed. Also a rectangular simply supported rectangular plate with $a/b = 2$, $h/b = 0.1$ and the same isotropic material properties as above has been analyzed considering an edge crack of different lengths d/b, inclination α and position c/a (see Fig. 2b). The corresponding results are listed in Table 7 where they are again compared with those presented in Ref [32]. Good agreement is observed between present and literature results for these benchmark cases. Finally, the case of through-

Table 6: Nondimensional frequency parameter λ for isotropic square plates with a central crack.

		Simply-supported						Cantilevered					
		$d/a = 0.2$		$d/a = 0.4$		$d/a = 0.6$		$d/a = 0.2$		$d/a = 0.4$		$d/a = 0.6$	
α	Mode	Present	Ref. [32]	Present	Ref. [32]	Present	Ref. [32]	Present	Ref. [32]	Present	Ref. [32]	Present	Ref. [32]
	1	5.58	5.58	5.23	5.23	4.91	4.91	1.04	1.04	1.04	1.04	1.03	1.03
	2	13.58	13.57	12.32	12.30	9.59	9.58	2.42	2.42	2.40	2.40	2.38	2.38
0°	3	13.75	13.74	13.64	13.62	13.36	13.35	6.08	6.08	6.08	6.07	5.89	6.01
	4	20.99	20.97	20.67	20.64	19.44	19.42	7.44	7.44	6.88	6.87	6.28	6.27
	5	24.15	24.12	22.08	22.05	20.83	20.81	8.53	8.52	8.39	8.39	7.91	7.90
	1	5.51	5.58	5.15	5.22	4.85	4.88	1.03	1.04	1.03	1.03	1.03	1.03
	2	13.45	13.57	12.32	12.30	9.52	9.58	2.39	2.42	2.37	2.39	2.34	2.35
15°	3	13.54	13.74	13.52	13.61	13.23	13.29	6.02	6.07	6.02	6.06	5.99	6.03
	4	20.65	20.94	20.25	20.40	19.21	19.30	7.32	7.46	6.68	6.91	6.18	6.31
	5	24.08	24.23	22.32	22.43	21.08	21.15	8.38	8.52	8.31	8.40	7.92	7.96
	1	5.52	5.58	5.18	5.21	4.80	4.82	1.03	1.04	1.02	1.03	1.01	1.02
	2	13.54	13.57	12.29	12.30	9.59	9.59	2.40	2.42	2.36	2.37	2.28	2.29
30°	3	13.59	13.74	13.50	13.58	13.11	13.16	6.02	6.04	5.98	5.99	5.83	5.93
	4	20.76	20.88	20.08	20.11	19.11	19.11	7.42	7.49	7.00	6.98	6.52	6.54
	5	24.41	24.39	23.12	23.15	21.07	21.05	8.47	8.53	8.40	8.44	8.10	8.73
	1	5.58	5.58	5.20	5.20	4.79	4.78	1.03	1.03	1.02	1.02	0.99	0.99
	2	13.58	13.57	12.31	12.29	9.61	9.59	2.42	2.42	2.36	2.36	2.26	2.24
45°	3	13.75	13.74	13.58	13.57	13.10	13.09	6.00	6.00	5.86	5.86	5.66	5.64
	4	20.87	20.85	20.01	19.99	19.05	19.03	7.54	7.55	7.21	7.22	6.86	6.80
	5	24.51	24.49	23.59	23.57	20.97	20.94	8.54	8.53	8.49	8.49	8.32	8.29

the-thickness cracked laminates is analyzed considering a square, clamped plate having thickness ratio $h/a = 0.1$ and central cracks ($c/a = e/a = 0.5$) with different length ratios d/a and inclination α. The $[0/90/45/-45/-45/45/90/0]$ and $[0/90/45/-45/45/-45/0/90]$ layups have been considered with straight fiber laminas exhibiting the same orthotropic material properties used in the preceding analyses. Table 8 lists the natural frequencies resulting from the analyses carried out, using the implemented code

Table 7: Nondimensional frequency parameter λ for isotropic rectangular plate ($a/b = 2$) with edge crack.

			$d/b = 0.2$		$d/b = 0.4$		$d/b = 0.6$	
α	c/a	Mode	Present	Ref. [32]	Present	Ref. [32]	Present	Ref. [32]
		1	14.56	14.59	14.42	14.48	14.12	14.20
		2	22.93	22.97	22.73	22.75	21.64	21.63
90°	0.5	3	36.52	36.65	35.42	35.77	33.45	33.86
		4	46.83	47.24	46.30	46.91	40.84	41.82
		5	54.67	54.68	51.83	52.08	46.37	46.84
		1	14.58	14.58	14.49	14.50	14.24	14.24
		2	23.00	23.03	22.58	22.65	21.66	21.75
90°	0.25	3	36.54	36.62	35.80	35.86	32.58	32.53
		4	47.18	47.12	46.70	46.91	42.40	42.97
		5	54.62	54.53	53.01	53.05	47.62	47.60
		1	14.55	14.55	14.28	14.27	13.66	13.66
		2	23.05	23.05	22.91	22.90	22.43	22.42
135°	0.25	3	36.62	36.62	36.00	35.98	33.71	3.42
		4	47.04	47.03	45.47	45.45	43.83	43.82
		5	54.67	54.65	53.31	53.29	49.97	49.93

with variable stiffness computing capabilities, and their comparison with results obtained by converged models in MSC Nastran® finite element code. Also for these analyses the comparison of present and reference results show very good agreement.

In conclusion, the presented convergence and accuracy studies allow to consider the proposed method and its computational implementation validated. The combination of its capabilities and features, verified by the analysis of uncracked variable stiffness plates and cracked constant stiffness plates, allows to be confident that the method can be successfully applied to investigate also cracked variable stiffness plates free vibrations that, to the best of the author's knowledge, have not been yet investigated and for which no data are available in the literature.

3.2 Application to cracked variable angle tow laminated plates

A general and comprehensive parametric study of cracked variable stiffness composite laminates is not feasible due to the huge number of different configurations that arise by considering the involved parameters (fiber deposition law, layup, crack position, crack length, crack inclination). On the basis of this observation, in this section an example study is presented to show the potentiality of the proposed approach and highlight some features of variable stiffness plates that can be useful in structural design. In particular, the VAT laminate configuration just used for some buckling studies in Refs. [34] and [24] is here investigated.

Table 8: Nondimensional frequency parameter λ for clamped cracked square laminates.

		$[0/90/45/-45/-45/45/90/0]$						$[0/90/45/-45/45/-45/0/90]$					
		$d/a=0.2$		$d/a=0.4$		$d/a=0.6$		$d/a=0.2$		$d/a=0.4$		$d/a=0.6$	
α	Mode	Present	FEM	Present	FEM	Present	FEM	Present	FEM	Present	FEM	Present	FEM
	1	4.30	4.30	4.17	4.17	4.07	4.07	4.26	4.22	4.10	4.06	3.99	3.95
	2	6.77	6.78	5.99	6.01	4.93	4.94	7.10	7.00	6.03	5.96	4.83	4.79
0°	3	7.77	7.77	7.73	7.73	7.66	7.66	7.35	7.24	7.30	7.20	7.22	7.12
	4	9.53	9.53	9.34	9.35	8.92	8.93	9.52	9.38	9.34	9.21	8.67	8.56
	5	9.99	9.99	9.51	9.52	9.13	9.14	10.69	10.53	10.09	9.95	9.76	9.62
	1	4.26	4.28	4.09	4.11	3.97	3.98	4.24	4.20	4.05	4.02	3.93	3.89
	2	6.75	6.80	5.97	5.99	4.86	4.88	7.10	7.00	5.97	5.92	4.80	4.76
30°	3	7.65	7.72	7.49	7.53	7.28	7.31	7.24	7.24	7.22	7.15	7.04	6.96
	4	9.39	9.51	9.23	9.27	8.96	8.97	9.13	9.37	9.31	9.23	8.81	8.71
	5	9.99	10.10	9.67	9.76	9.04	9.11	10.61	10.60	10.20	10.10	9.45	9.32
	1	4.27	4.27	4.07	4.07	3.94	3.94	4.25	4.20	4.05	4.01	3.92	3.88
	2	6.82	6.83	5.97	5.99	4.84	4.85	7.09	7.00	5.97	5.91	4.80	4.76
45°	3	7.64	7.64	7.29	7.30	7.04	7.04	7.34	7.23	7.23	7.13	7.01	6.92
	4	9.50	9.50	9.27	9.27	8.82	8.83	9.51	9.37	9.37	9.24	9.10	8.97
	5	10.18	10.19	9.96	9.96	9.35	9.36	10.79	10.63	10.27	10.14	9.12	9.01
	1	4.25	4.26	4.06	4.06	3.92	3.93	4.24	4.20	4.06	4.02	3.93	3.90
	2	6.86	6.87	5.98	6.01	4.79	4.81	7.07	7.00	5.97	5.92	4.79	4.76
60°	3	7.52	7.56	7.07	7.09	6.85	6.87	7.29	7.24	7.24	7.15	7.03	6.96
	4	9.45	9.51	9.24	9.28	8.58	8.62	9.42	9.37	9.35	9.23	8.79	8.72
	5	10.25	10.28	10.12	10.17	9.76	9.78	10.70	10.60	10.23	10.10	9.44	9.32
	1	4.25	4.25	4.06	4.06	3.93	3.93	4.26	4.22	4.10	4.06	3.99	3.95
	2	6.94	6.94	6.01	6.03	4.73	4.75	7.10	7.00	6.03	5.96	4.83	4.79
90°	3	7.41	7.43	6.89	6.89	6.77	6.77	7.35	7.24	7.30	7.20	7.22	7.12
	4	9.53	9.53	9.28	9.29	8.36	8.38	9.52	9.38	9.34	9.21	8.67	8.56
	5	10.35	10.35	10.28	10.28	10.25	10.26	10.69	10.53	10.09	9.95	9.76	9.62

It is a square plate having $a = b = 0.24\,\mathrm{m}$ and $[0 \pm \langle \vartheta_A/\vartheta_B \rangle]_{3S}$ layup (see C for VAT laminate notation and fiber pattern definition). Each fibre reinforced ply is 0.127 mm thick and presents a linear variation of the fiber deposition angle as per Eq. (19) where ϑ_A and ϑ_B are evaluated at the center and at the edge of the ply, respectively. The plies have the following material properties in the orthotropic reference system: $E_1 = 181.0\,\mathrm{GPa}$, $E_2 = 10.3\,\mathrm{GPa}$, $G_{31} = 7.0\,\mathrm{GPa}$, $G_{32} = 3.0\,\mathrm{GPa}$, $G_{12} = 7.17\,\mathrm{GPa}$, $\nu_{12} = 0.28$ and $\rho = 1540.0\,\mathrm{kg\,m^{-3}}$. Two sets of boundary conditions have been considered, namely simply-supported and clamped edges. Furthermore, analyses for both an embedded crack (Fig. 2a) and an edge crack (Fig. 2b) have been carried out assuming different lengths d and inclination α. The results presented in the following have been obtained by setting $N = 16$ and $N_c = 5$ in the approximation scheme, that provides converged results as per preliminary convergence analyses. In the discussion, the focus is on the first vibration mode, nevertheless the developed tool is obviously able to provide results and to enable similar investigations also for the other vibrations modes.

3.3 Embedded central crack

In this subsection the case of an embedded central crack ($c/a = e/a = 0.5$ as defined in Fig. 2a) is discussed considering different values of the crack length d and inclination α. Figs. 3 and 4 show the first mode nondimensional frequency variation with respect to the laminate fiber deposition characteristic angles, namely ϑ_A and ϑ_B, for the simply supported and clamped boundary conditions, respectively. Each figure reports by columns the plots for fixed crack length and by rows the plots for fixed crack inclinations. Analysis of the results returns the following general considerations. As expected, the plate natural frequency decreases for the presence of the crack as this reduces the plate stiffness; this effect is more and more pronounced as the crack length grows. The crack inclination determines variations in the vibration frequency that are stronger for the lower and higher values of ϑ_A and ϑ_B, as shown by the exemplificative curves of Fig. 5, whereas fibre patterns with intermediate values of the characteristics angles have lesser sensitivity with respect to this parameter. Moreover, for a given crack configuration, the modal shape is influenced by the fibres pattern; this effect is not marked at global level but concentrates in the crack zone where different crack opening arise evidencing possible modifications in the crack mode mixing. To illustrate this occurrence, Fig. 6 reports the first mode transverse displacement distributions corresponding to different fibre path angles ϑ_A and ϑ_B when a central crack with $d/a = 0.4$ and $\alpha = 45°$ is considered. To better detail with an example, Fig. 7 compares the deformed modal shapes of the

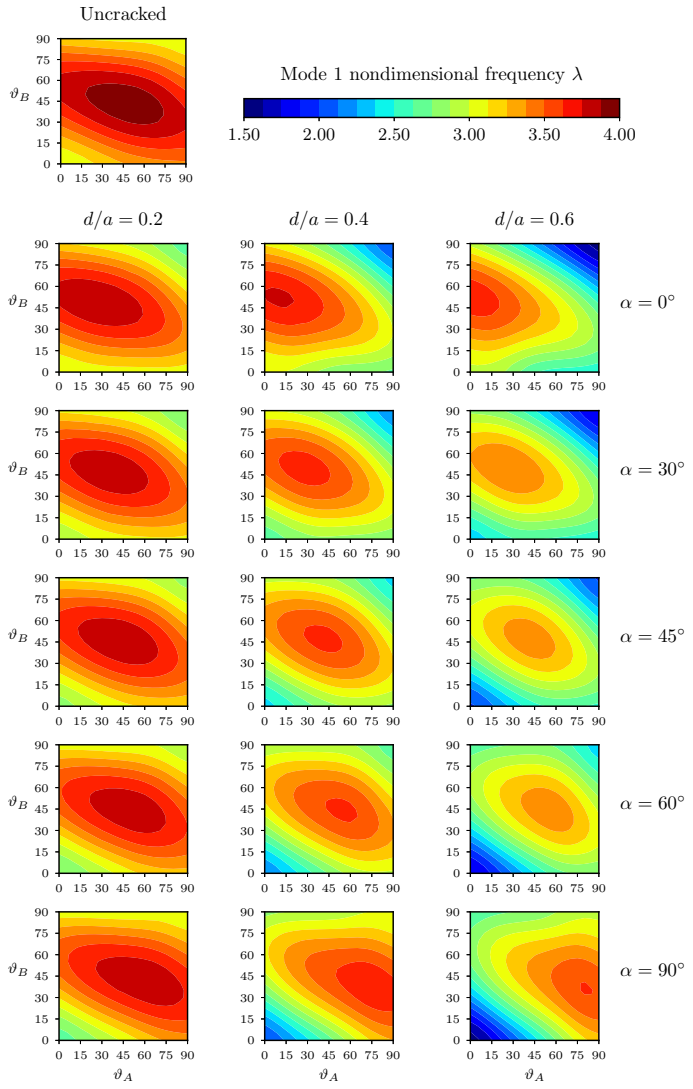

Figure 3: First mode nondimensional frequency λ for the $[0 \pm \langle \vartheta_A / \vartheta_B \rangle]_{3S}$ VAT simply supported square laminate containing a central crack ($c/a = e/a = 0.5$) with different lengths d and inclinations *alpha*.

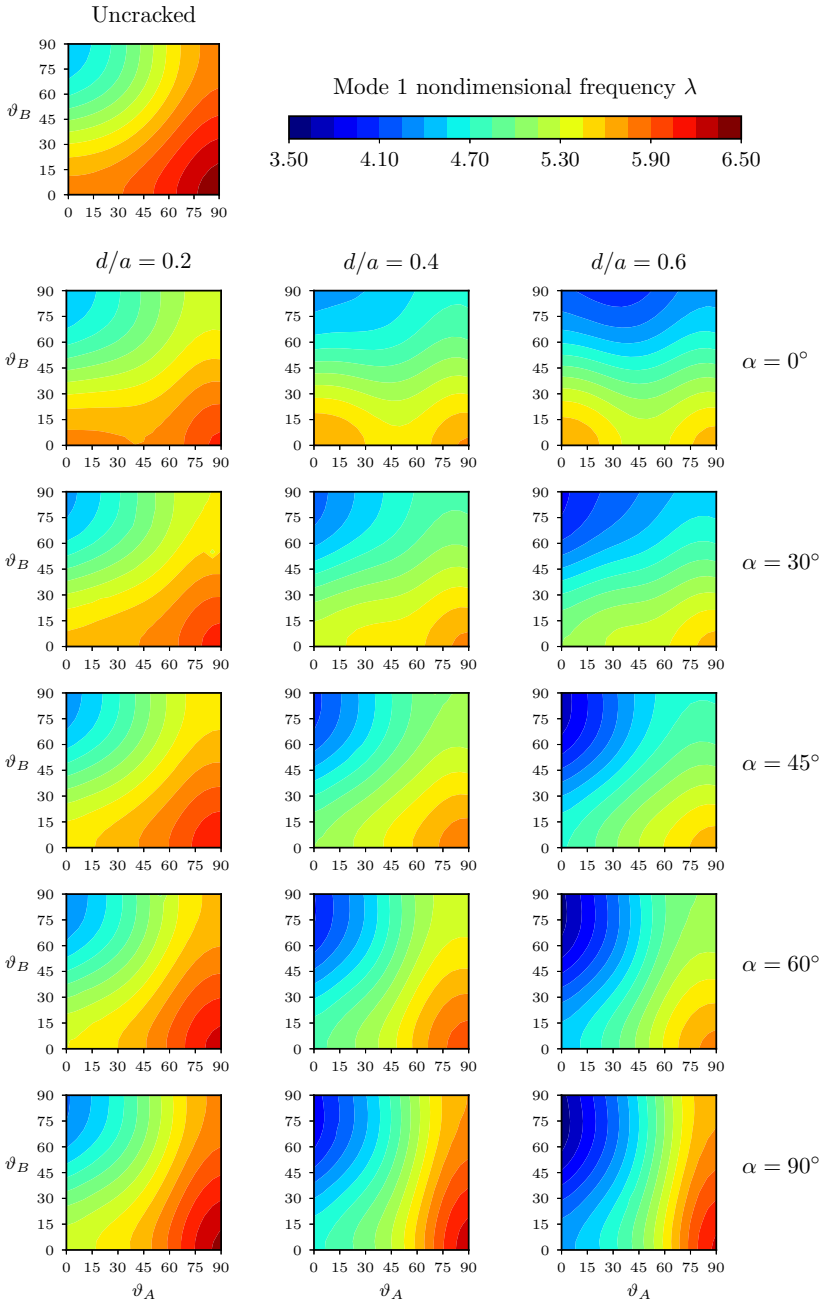

Figure 4: First mode nondimensional frequency λ for the $[0 \pm \langle \vartheta_A/\vartheta_B \rangle]_{3S}$ VAT clamped square laminate containing a central crack ($c/a = e/a = 0.5$) with different lengths d and inclinations *alpha*.

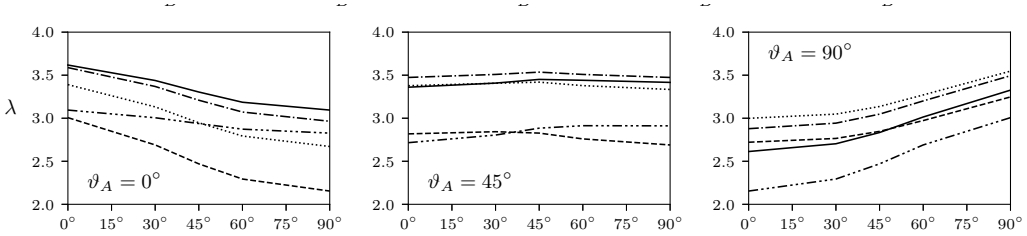

(a) Simply supported laminate.

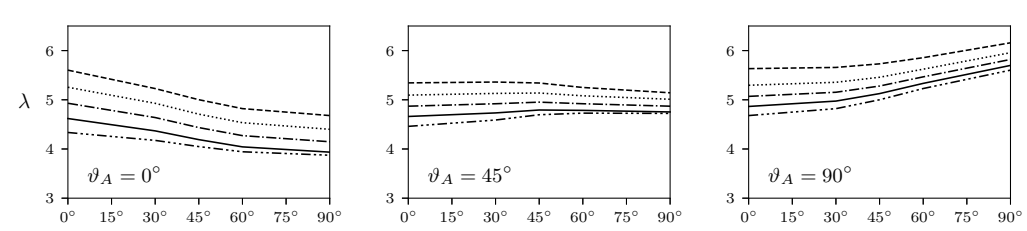

(b) Clamped laminate.

Figure 5: First mode nondimensional frequency λ variation with respect to crack inclination α for the $[0 \pm \langle \vartheta_A/\vartheta_B \rangle]_{3S}$ VAT laminate with a central crack ($c/a = e/a = 0.5$) having $d/a = 0.6$.

laminates with $(\vartheta_A, \vartheta_B) = (90°, 60°)$ and $(\vartheta_A, \vartheta_B) = (45°, 0°)$.

A useful investigation for design concerns the sensitivity of the cracked plate vibration frequencies as the fiber deposition path varies. Figs. 8 and 9 show the percentage variation of the plate fundamental frequency, denoted by $\Delta\lambda\%$, with respect to that of the corresponding straight fibres ($\vartheta_A = \vartheta_B$) cracked plate for the simply supported and clamped laminates, respectively. In particular, each plot of the figures refers to a given crack configuration in terms of length and inclination and reports $\Delta\lambda\%$ as function of the fiber path angle ϑ_B, assuming that the fiber path angle ϑ_A is fixed. Data analysis evidences that for a given crack configuration it could be possible to find fibres paths with $\Delta\lambda\% > 0$, which then enable the possibility to keep down the plate stiffness loss with respect to the straight fibres case. Some explanatory examples are provided for the simply supported plate case (refer to Fig. 8):

– if $d/a = 0.6$ and $\alpha = 30°$, for $\vartheta_A = 90°$ all the VAT fibres pattern reduce the loss in stiffness with respect to the straight fiber case, whereas for $\vartheta_A = 45°$ the straight fibres laminate provides the higher stiffness;

– if $d/a = 0.4$ and $\alpha = 45°$, assuming $\vartheta_A = 60°$ there is a slight stiffness improvement for $20° < \vartheta_B < 65°$, whereas for $\vartheta_A < 0°$ all the fibres paths provide higher vibration frequency than the straight fibres case;

– if $d/a = 0.2$ and $\alpha = 30°$, assuming $\vartheta_B = 75°$, values $30° \widetilde{<} \vartheta_A < 75°$ determine loss in stiffness greater than straight fibers.

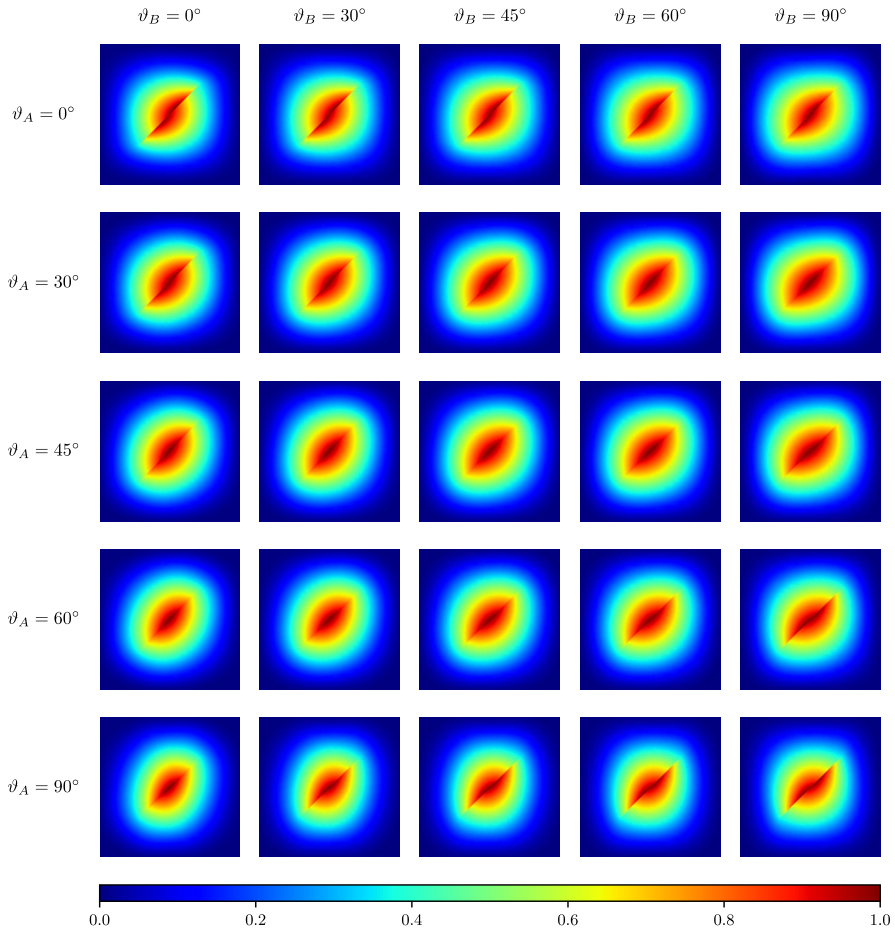

Figure 6: First mode shape for the $[0 \pm \langle \vartheta_A / \vartheta_B \rangle]_{3S}$ VAT clamped square laminates containing an embedded crack with $d/a = 0.6$, $c/a = e/a = 0.5$ and $\alpha = 45°$. Color fringes represent constant values of u_3/u_{3max}.

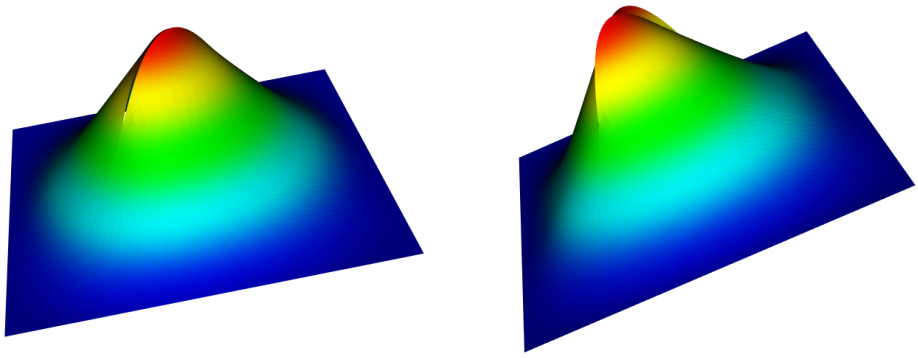

(a) $[0 \pm \langle 45^\circ/0^\circ \rangle]_{3S}$ VAT laminate (b) $[0 \pm \langle 90^\circ/60^\circ \rangle]_{3S}$ VAT laminate

Figure 7: First mode deformation for VAT clamped square laminates containing an embedded crack with $d/a = 0.6$, $c/a = e/a = 0.5$ and $\alpha = 45^\circ$. Color fringes represent constant values of transverse displacement.

Similarly, other examples are provided for the clamped boundary conditions (refer to Fig. 9):

– if $d/a = 0.4$ and $\alpha = 60^\circ$, if $\vartheta_B < \vartheta_A$ there is a gain in the sense that the frequency reduction is lower than that of the straight fiber case;

– if $d/a = 0.2$ and $\alpha = 45^\circ$, for a given ϑ_B angles $\vartheta_A > \vartheta_B$ determines vibration frequency higher than the corresponding straight fiber laminate.

As showed by the previous examples, the stiffness loss and then the natural frequency variation for cracked VAT plates depend on crack parameters, fibres patterns and boundary conditions. For damage tolerant design, this makes crucial the detailed investigations of free vibrations for which the present approach propose itself as an efficient and versatile analysis tool.

3.4 Edge crack

To complete the illustration of the proposed approach the case of edge cracks is briefly examined in this subsection. Supported by many analyses carried out, not fully reported here for the sake of brevity, observations and conclusions similar to those presented in the preceding subsection for the embedded crack hold. In the following, some exemplifying results for laminates with the same characteristics as those of the preceding section but containing an edge crack with $c/a = 0.5$ and different lengths d and inclinations α (see Fig. 2b) are given to support the method capabilities. For the simply supported boundary conditions case, Fig. 10 shows the first mode nondimensional frequency distribution with

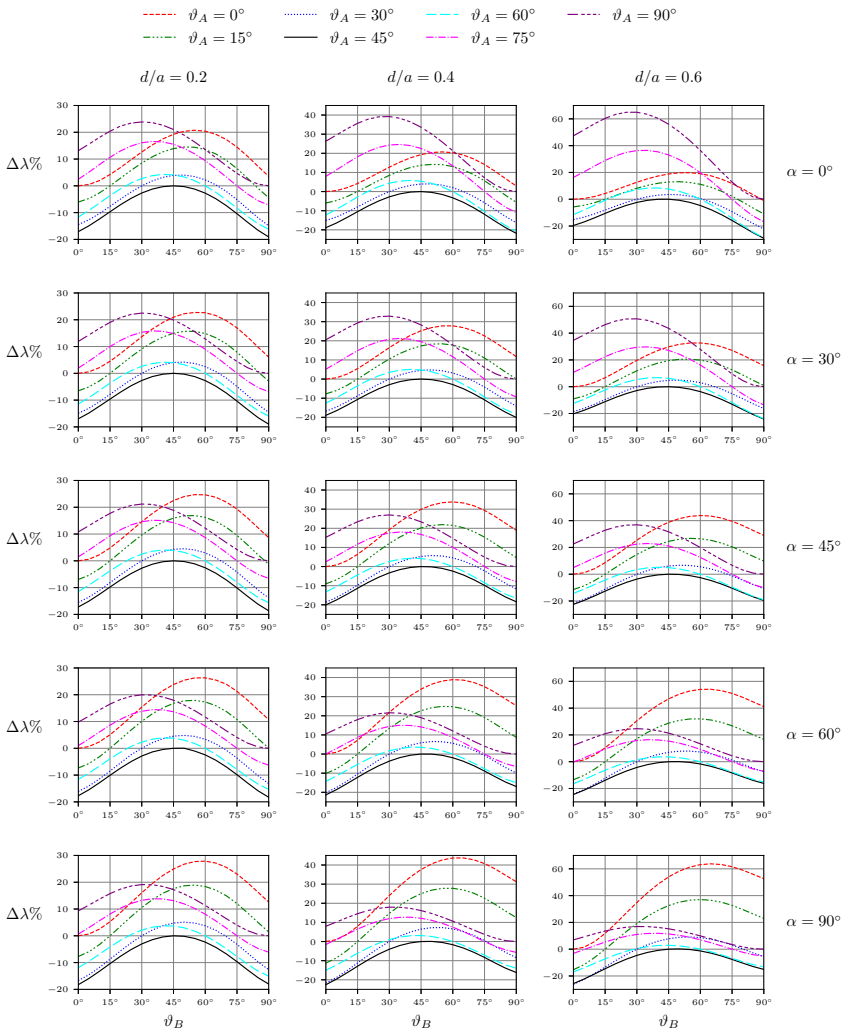

Figure 8: Percentage first mode nondimensional frequency λ reduction for the $[0 \pm \langle \vartheta_A / \vartheta_B \rangle]_{3S}$ VAT simply supported square laminate containing a central crack with different lengths and inclinations.

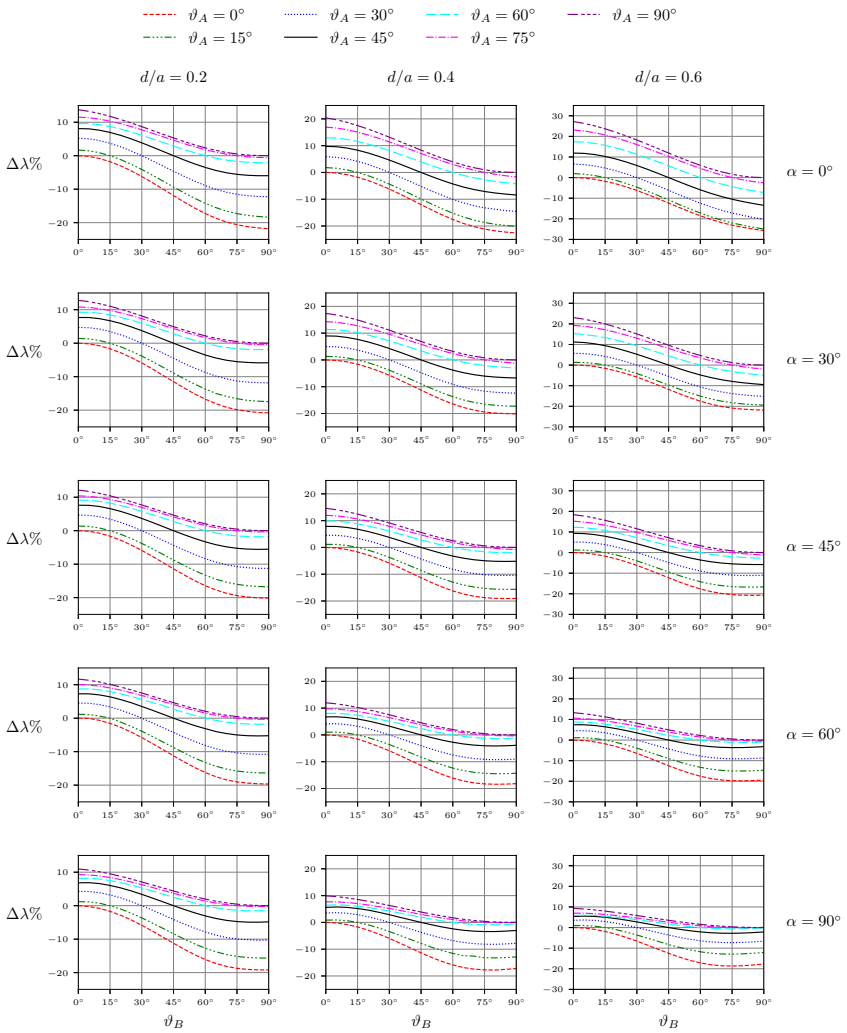

Figure 9: Percentage first mode nondimensional frequency λ reduction for the $[0 \pm \langle \vartheta_A/\vartheta_B \rangle]_{3S}$ VAT clamped square laminate containing a central crack with different lengths and inclinations.

respect to the fiber deposition path characteristic angles ϑ_A and ϑ_B. Fig. 6 illustrates the modal shape variations for the laminate containing an edge crack with $d/a = 0.4$ and $\alpha = 120°$.

4 Conclusions

A single-domain, meshless method for the free vibrations analysis of cracked variable stiffness composite plates and corresponding results have been presented. Known in the literature as eXtended Ritz or X–Ritz method, this approach is based on the pb2 Ritz method coupled with the employement as trial functions of both standard orthogonal polynomials and special functions, which are able to inherently account for displacement discontinuity and crack tip singular fields. Considering that, to the best of the author's knowledge, this is the first study on free vibrations of variable stiffness cracked composite plates, an extensive validation activity has been carried out and convergence characteristics and accuracy of the method have been ascertained by comparison with literature data on cracked isotropic plates and uncracked variable stiffness plates. Representative case studies for variable angle tow laminated plates, with different crack lengths, inclinations and plate boundary conditions, have been presented and discussed. The obtained results evidence the effects of the fibre patterns on the vibration frequency and modal shapes of variable angle tow laminates. They indicate that the stiffness loss due to the crack presence can be reduced to a certain extent by properly choosing the fibre path. This opens to alternative and viable solutions in the framework of damage tolerant design of composite structures.

5 Acknowledgment

The author would like to acknowledge the DEVISU project, supported by the Ministero dell'Istruzione, dell'Universitá della Ricerca research funding programme PRIN 2017.

References

[1] B. Sobhani Aragh, E. Borzabadi Farahani, B.X. Xu, H. Ghasemnejad, and W.J. Mansur. Manufacturable insight into modelling and design considerations in fibre-steered composite laminates: State of the art and perspective. *Computer Methods in Applied Mechanics and Engineering*, 379, 2021.

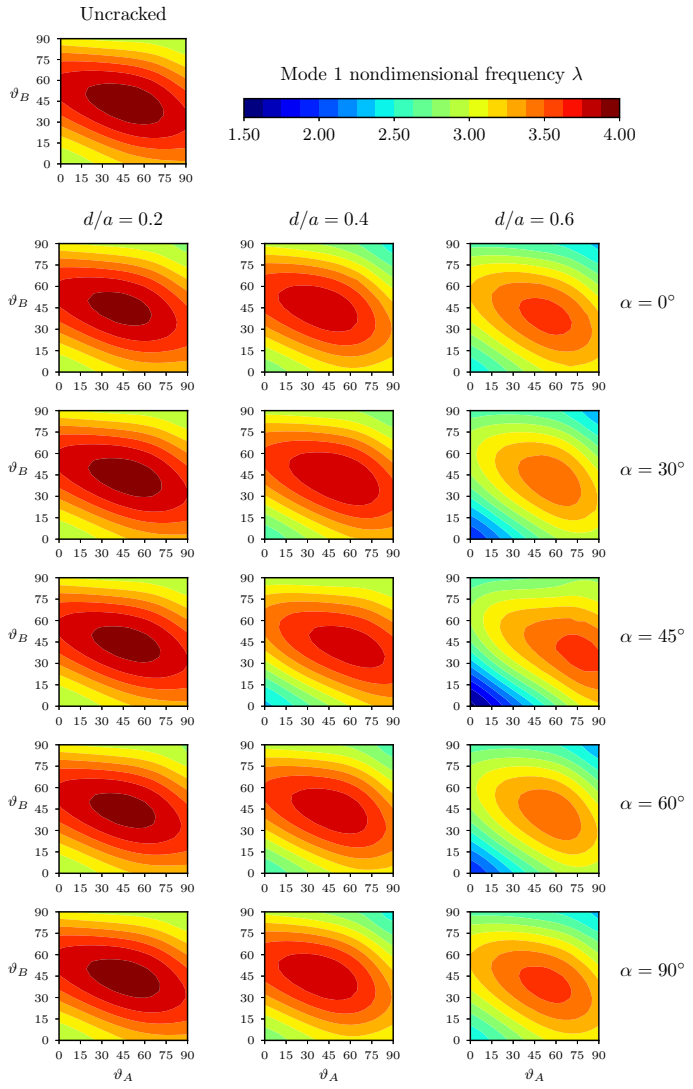

Figure 10: First mode nondimensional frequency λ for the $[0 \pm \langle \vartheta_A / \vartheta_B \rangle]_{3S}$ VAT simply supported square laminate containing an edge crack ($c/a = 0.5$) with different lengths d and inclinations α.

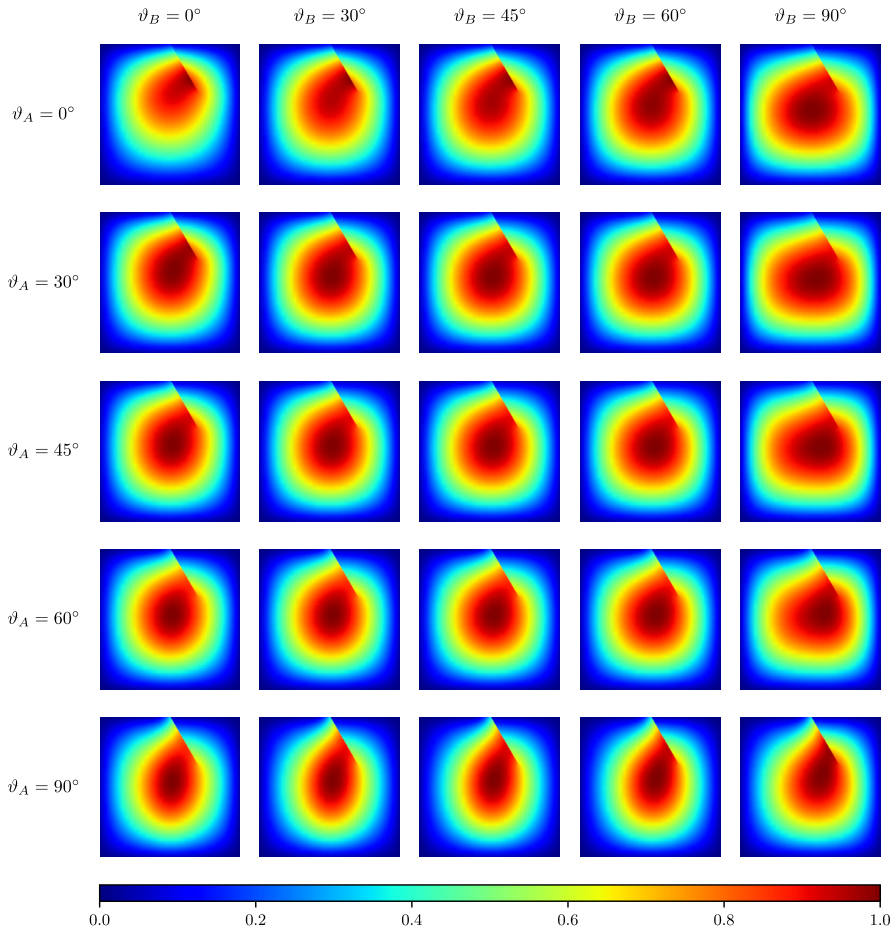

Figure 11: First mode shape for the $[0 \pm \langle \vartheta_A / \vartheta_B \rangle]_{3S}$ VAT simply supported square laminates containing an edge crack with $c/a = 0.5$, $d/a = 0.4$ and $\alpha = 120°$. Color fringes represent constant values of u_3/u_{3max}.

[2] P. Ribeiro, H. Akhavan, A. Teter, and J. Warmiński. A review on the mechanical behaviour of curvilinear fibre composite laminated panels. *Journal of Composite Materials*, 48(22):2761–2777, 2014.

[3] M.M. Abdalla, S. Setoodeh, and Z. Gürdal. Design of variable stiffness composite panels for maximum fundamental frequency using lamination parameters. *Composite Structures*, 81(2):283–291, 2007.

[4] A. Guenanou and A. Houmat. Free vibration analysis of symmetrically laminated composite circular plates with curvilinear fibers. *Science and Engineering of Composite Materials*, 24(1):111–121, 2017.

[5] W. Zhao and R.K. Kapania. Prestressed vibration of stiffened variable-angle tow laminated plates. *AIAA Journal*, 57(6):2575–2593, 2019.

[6] M. Hachemi, S.M. Hamza-Cherif, and A. Houmat. Free vibration analysis of variable stiffness composite laminate plate with circular cutout. *Australian Journal of Mechanical Engineering*, 18(1):63–79, 2020.

[7] M. Hachemi and A. Guenanou. Effect of the fiber orientation angle on the vibrational behavior of symmetric and antisymmetric vslc elliptical plates. *Mechanics Based Design of Structures and Machines*, 2020.

[8] Narayan Sharma, Prasant Kumar Swain, D. K. Maiti, and B. N. Singh. Stochastic frequency analysis of laminated composite plate with curvilinear fiber. *Mechanics of Advanced Materials and Structures*, 0(0):1–16, 2020.

[9] S. Yazdani and P. Ribeiro. A layerwise p-version finite element formulation for free vibration analysis of thick composite laminates with curvilinear fibres. *Composite Structures*, 120:531–542, 2015.

[10] H. Akhavan and P. Ribeiro. Natural modes of vibration of variable stiffness composite laminates with curvilinear fibers. *Composite Structures*, 93(11):3040–3047, 2011.

[11] Y. Yan, B. Liu, Y. Xing, E. Carrera, and A. Pagani. Free vibration analysis of variable stiffness composite laminated beams and plates by novel hierarchical differential quadrature finite elements. *Composite Structures*, 274, 2021. cited By 1.

[12] A. Houmat. Three-dimensional free vibration analysis of variable stiffness laminated composite rectangular plates. *Composite Structures*, 194:398–412, 2018.

[13] P. Ribeiro and H. Akhavan. Non-linear vibrations of variable stiffness composite laminated plates. *Composite Structures*, 94(8):2424–2432, 2012.

[14] H. Akhavan and P. Ribeiro. Free geometrically nonlinear oscillations of perfect and imperfect laminates with curved fibres by the shooting method. *Nonlinear Dynamics*, 81(1-2):949–965, 2015.

[15] B. Daraei and S. Hatami. Free vibration analysis of variable stiffness composite laminates with flat and folded shapes. *Journal of Solid Mechanics*, 8(3):662–678, 2016.

[16] G. Nie, H. Hu, Z. Zhong, and X. Chen. A complex fourier series solution for free vibration of arbitrary straight-sided quadrilateral laminates with variable angle tows. *Mechanics of Advanced Materials and Structures*, 2020.

[17] Y. Heydarpour and M.M. Aghdam. A hybrid bézier based multi-step method and differential quadrature for 3d transient response of variable stiffness composite plates. *Composite Structures*, 154:344–359, 2016.

[18] Shinya Honda, Yoshihiro Narita, and Katsuhiko Sasaki. Maximizing the fundamental frequency of laminated composite plates with optimally shaped curvilinear fibers. *Journal of System Design and Dynamics*, 3(6):867–876, 2009.

[19] D.A. Pereira, T.A.M. Guimarães, H.B. Resende, and D.A. Rade. Numerical and experimental analyses of modal frequency and damping in tow-steered cfrp laminates. *Composite Structures*, 244:112190, 2020.

[20] Riccardo Vescovini and Lorenzo Dozio. A variable-kinematic model for variable stiffness plates: Vibration and buckling analysis. *Composite Structures*, 142:15–26, 2016.

[21] A. Milazzo, I. Benedetti, and V. Gulizzi. An extended Ritz formulation for buckling and post-buckling analysis of cracked multilayered plates. *Composite Structures*, 201:980–994, 2018.

[22] A. Milazzo, I. Benedetti, and V. Gulizzi. A single-domain Ritz approach for buckling and post-buckling analysis of cracked plates. *International Journal of Solids and Structures*, 159:221–231, 2019.

[23] V. Gulizzi, V. Oliveri, and A. Milazzo. Buckling and post-buckling analysis of cracked stiffened panels via an X-Ritz method. *Aerospace Science and Technology*, 86:268–282, 2019.

[24] A. Milazzo and V. Oliveri. Investigation of buckling characteristics of cracked variable stiffness composite plates by an eXtended Ritz approach. *Thin-Walled Structures*, 163, 2021.

[25] A. Milazzo and V. Oliveri. Post-buckling analysis of cracked multilayered composite plates by pb-2 Rayleigh-Ritz method. *Composite Structures*, 132:75–86, 2015.

[26] J.N. Reddy. *Mechanics of laminated composite plates and shells. Theory and analysis.* CRC Press, 2004.

[27] J.N. Reddy. *Energy Principles and Variational Methods in Applied Mechanics.* John Wiley & Sons, 2002.

[28] K. M. Liew and C. M. Wang. pb-2 Rayleigh - Ritz method for general plate analysis. *Engineering Structures*, 15(1):55–60, January 1993.

[29] M.V.V. Murthy, K.N. Raju, and S. Viswanath. On the bending stress distribution at the tip of a stationary crack from reissner's theory. *International Journal of Fracture*, 17(6):537–552, 1981.

[30] A. T. Zehnder and M. J. Viz. Fracture mechanics of thin plates and shells under combined membrane, bending, and twisting loads. *Applied Mechanics Reviews*, 58(1):37–48, 2005.

[31] C.S. Huang and A.W. Leissa. Vibration analysis of rectangular plates with side cracks via the Ritz method. *Journal of Sound and Vibration*, 323(3-5):974–988, 2009.

[32] C.S. Huang, A.W. Leissa, and R.S. Li. Accurate vibration analysis of thick, cracked rectangular plates. *Journal of Sound and Vibration*, 330(9):2079–2093, 2011.

[33] C.S. Huang, A.W. Leissa, and C.W. Chan. Vibrations of rectangular plates with internal cracks or slits. *International Journal of Mechanical Sciences*, 53(6):436–445, 2011.

[34] Z. Gürdal, B.F. Tatting, and C.K. Wu. Variable stiffness composite panels: Effects of stiffness variation on the in-plane and buckling response. *Composites Part A: Applied Science and Manufacturing*, 39(5):911–922, 2008.

[35] Sailendra N. Chatterjee and Satish V. Kulkarni. Shear correction factors for laminated plates. *AIAA Journal*, 17(5):498–499, 1979.

A Plate section stiffness properties

Assuming a plane stress state, namely $\sigma_{33} = 0$, the material behaviour at the plate point of coordinates (x_1, x_2, x_3) is given by the generalized orthotropic constitutive law

$$\boldsymbol{\sigma} = \left\{ \begin{array}{c} \boldsymbol{\sigma}_p \\ \hline \boldsymbol{\sigma}_n \end{array} \right\} = \left\{ \begin{array}{c} \sigma_{11} \\ \sigma_{22} \\ \sigma_{12} \\ \hline \sigma_{31} \\ \sigma_{32} \end{array} \right\} = \left[\begin{array}{ccc|cc} Q_{11} & Q_{12} & Q_{13} & 0 & 0 \\ Q_{12} & Q_{22} & Q_{23} & 0 & 0 \\ Q_{13} & Q_{23} & Q_{33} & 0 & 0 \\ \hline 0 & 0 & 0 & Q_{44} & Q_{45} \\ 0 & 0 & 0 & Q_{45} & Q_{55} \end{array} \right] \left\{ \begin{array}{c} \varepsilon_{11} \\ \varepsilon_{22} \\ \varepsilon_{12} \\ \hline \varepsilon_{31} \\ \varepsilon_{32} \end{array} \right\} = \left[\begin{array}{c|c} \boldsymbol{Q}_p & \boldsymbol{0} \\ \hline \boldsymbol{0} & \boldsymbol{Q}_n \end{array} \right] \left\{ \begin{array}{c} \boldsymbol{\varepsilon}_p \\ \hline \boldsymbol{\varepsilon}_n \end{array} \right\} = \boldsymbol{Q}\boldsymbol{\varepsilon} \tag{11}$$

where σ_{ij} are the stresses and ε_{ij} are the strains. Accordingly, the plate section stiffness matrices appearing in Eq. (1) are defined as

$$\boldsymbol{A}(x_1, x_2) = \int_h \boldsymbol{Q}_p(x_1, x_2, x_3)\ dx_3 \tag{12}$$

$$\boldsymbol{B}(x_1, x_2) = \int_h x_3\ \boldsymbol{Q}_p(x_1, x_2, x_3)\ dx_3 \tag{13}$$

$$\boldsymbol{D}(x_1, x_2) = \int_h x_3^2\ \boldsymbol{Q}_p(x_1, x_2, x_3)\ dx_3 \tag{14}$$

$$\boldsymbol{G}(x_1, x_2) = \boldsymbol{F} \int_h \boldsymbol{Q}_n(x_1, x_2, x_3)\ dx_3 \tag{15}$$

where $h = h(x_1, x_2)$ is the plate thickness and $\boldsymbol{F}$ is a 2×2 matrix containing the shear correction factors [35].

B Plate section inertia properties

The plate section inertia properties appearing in Eq. (1) are defined as

$$\boldsymbol{J}_0 = \int_h \rho\ \boldsymbol{I}_3\ dx_3 \tag{16}$$

$$\boldsymbol{J}_1 = \int_h \rho\ x_3\ \boldsymbol{\mathscr{L}}\ dx_3 \tag{17}$$

$$\boldsymbol{J}_2 = \int_h \rho\ x_3^2\ \boldsymbol{I}_2\ dx_3 \tag{18}$$

where ρ is the mass mass density and $\boldsymbol{I}_k$ denotes the $k \times k$ identity matrix.

C VAT laminates

Variable angle tow (VAT) laminates are plates obtained by stacking fiber-reinforced composite plies having fibres laid at a variable angle in the lamina plane. For VAT plies, the fibre orientation angle ϑ varies as a function of the in-plane coordinates, namely $\vartheta = \vartheta(x_1, x_2)$. Consequently, in VAT laminates the extensional stiffness matrix $\boldsymbol{A}$, the bending–extensional stiffness matrix $\boldsymbol{B}$, the bending stiffness matrix $\boldsymbol{D}$ and the shear stiffness matrix $\boldsymbol{G}$ are function of the plate in-plane coordinates x_1 and x_2; thus, VAT laminates are variable stiffness plates.

Referring to Fig.12, for the VAT plies considered in the present work, the angle ϑ varies according to the following law holding along the baseline $\mathbf{r}$

$$\vartheta = \vartheta_0 + \frac{\vartheta_A r_B - \vartheta_B r_A}{r_B - r_A} + |r| \, \frac{\vartheta_B - \vartheta_A}{r_B - r_A} \tag{19}$$

where ϑ_0 is the inclination of the baseline with respect to the x_1 axis, ϑ_A and ϑ_B are the fibre angles with respect to the baseline at the distances r_A and r_B from the projection O' of the plate center on the baseline. According to Gurdal [34], assuming that the point A corresponds to the origin of r, namely $r_A = 0$, and fixing $r_B - r_A = r_B = d$, such a fiber path is denoted by $\vartheta_0 + \langle \vartheta_A | \vartheta_B \rangle$. For a point of a VAT

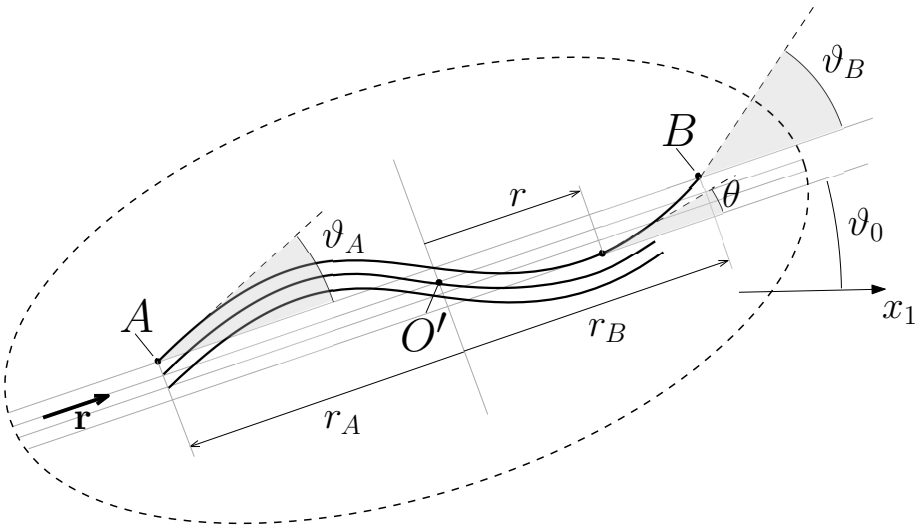

Figure 12: VAT parameter definitions.

ply having fibre deposition angle ϑ the stiffness properties are expressed as

$$Q_{11} = \bar{Q}_{11} \cos^4 \vartheta + 2 \left(\bar{Q}_{12} + 2\bar{Q}_{66} \right) \sin^2 \vartheta \cos^2 \vartheta + \bar{Q}_{22} \sin^4 \vartheta \tag{20a}$$

$$Q_{12} = \bar{Q}_{12}\cos^4\vartheta + \left(\bar{Q}_{11} + Q_{22} - 4\bar{Q}_{66}\right)\sin^2\vartheta\cos^2\vartheta + \bar{Q}_{12}\sin^4\vartheta \tag{20b}$$

$$Q_{22} = \bar{Q}_{11}\sin^4\vartheta + 2\left(\bar{Q}_{12} + 2\bar{Q}_{66}\right)\sin^2\vartheta\cos^2\vartheta + \bar{Q}_{22}\cos^4\vartheta \tag{20c}$$

$$Q_{16} = \left(\bar{Q}_{11} - Q_{12} - 2\bar{Q}_{66}\right)\sin\vartheta\cos^3\vartheta + \left(\bar{Q}_{12} - Q_{22} + 2\bar{Q}_{66}\right)\sin^3\vartheta\cos\vartheta \tag{20d}$$

$$Q_{26} = \left(\bar{Q}_{11} - Q_{12} - 2\bar{Q}_{66}\right)\sin^3\vartheta\cos\vartheta + \left(\bar{Q}_{12} - Q_{22} + 2\bar{Q}_{66}\right)\sin\vartheta\cos^3\vartheta \tag{20e}$$

$$Q_{66} = \left(\bar{Q}_{11} + Q_{22} - 2\bar{Q}_{12} - 2\bar{Q}_{66}\right)\sin^2\vartheta\cos^2\vartheta + \bar{Q}_{66}\left(\sin^4\vartheta + \cos^4\vartheta\right)\cos\vartheta \tag{20f}$$

$$Q_{44} = \bar{Q}_{44}\cos^2\vartheta + \bar{Q}_{55}\sin^2\vartheta \tag{20g}$$

$$Q_{45} = \left(\bar{Q}_{55} - \bar{Q}_{44}\right)\cos\vartheta\sin\vartheta \tag{20h}$$

$$Q_{55} = \bar{Q}_{44}\sin^2\vartheta + \bar{Q}_{55}\cos^2\vartheta \tag{20i}$$

where

$$\bar{Q}_{11} = \frac{E_1}{1 - \nu_{12}\nu_{21}} \tag{21a}$$

$$\bar{Q}_{22} = \frac{E_2}{1 - \nu_{12}\nu_{21}} \tag{21b}$$

$$\bar{Q}_{12} = \frac{\nu_{12}E_2}{1 - \nu_{12}\nu_{21}} \tag{21c}$$

$$\bar{Q}_{66} = G_{12} \tag{21d}$$

$$\bar{Q}_{44} = G_{23} \tag{21e}$$

$$\bar{Q}_{44} = G_{13} \tag{21f}$$

being E_i the Young moduli, G_{ij} the shear moduli and ν_{ij} the Poisson's coefficients measured in the material orthotropic reference frame .